Inorganic Chemistry

Article

pubs.acs.org/IC

High-Pressure Synthesis, Crystal Structures, and Properties of $ScRhO_3$ and $InRhO_3$ Perovskites

Alexei A. Belik,*[,†] Yoshitaka Matsushita,[‡] Masahiko Tanaka,[‡] and Eiji Takayama-Muromachi[§]

[†]International Center for Materials Nanoarchitectonics (WPI-MANA), National Institute for Materials Science (NIMS), 1-1 Namiki, Tsukuba, Ibaraki 305-0044, Japan

[‡]SPring-8 Office, NIMS, Kohto 1-1-1, Sayo-cho, Hyogo 679-5148, Japan

[§]National Institute for Materials Science (NIMS), 1-2-1 Sengen, Tsukuba, Ibaraki 305-0047, Japan

Supporting Information

ABSTRACT: $ScRhO_3$ and $InRhO_3$ perovskites were synthesized at a high pressure of 6 GPa and a high temperature of 1500 K. Crystal structures of $ScRhO_3$ and $InRhO_3$ were studied with synchrotron X-ray powder diffraction at 293 and 134 K. $ScRhO_3$ and $InRhO_3$ have a rarely observed monoclinic superstructure of the $GdFeO_3$-type structure (space group $P2_1/n$, a = 7.45660 Å, b = 7.43524 Å, c = 7.52191 Å, and β = 93.2930° for $ScRhO_3$ and a = 7.59020 Å, b = 7.58377 Å, c = 7.59010 Å, and β = 91.4154° for $InRhO_3$ at 293 K). $InRhO_3$ has pseudo-orthorhombic lattice parameters of a = 10.8658 Å, b = 7.5837 Å, and c = 10.6006 Å. $ScRhO_3$ and $InRhO_3$ are nonmagnetic, and no phase transitions were detected between 2 and 873 K. Crystallographic trends and distortions of $ScRhO_3$, $InRhO_3$, and $RRhO_3$ (R = rare earths, Y, and Bi) are discussed.

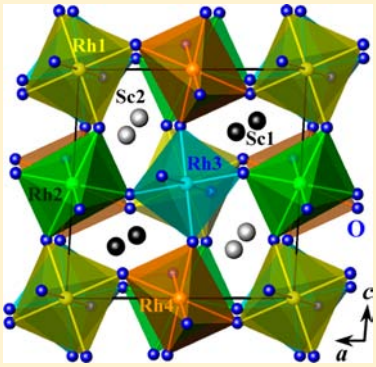

1. INTRODUCTION

ABO_3 perovskites form a very large and important class of compounds and materials.[1] The stability and distortions of perovskites are often understood using the Goldschmidt tolerance factor,[2] $t = (r_A + r_O)/[2^{1/2}(r_B + r_O)]$, where r_A, r_B, and r_O are the ionic radii of the A, B, and oxygen ions, respectively, in perovskite ABO_3. The perovskite structure is stable within the limits of t between 0.77 and 0.99 if the A and B ionic radii are based on octahedral coordination.[3] Therefore, the A site of perovskites is usually occupied by large cations such as rare earth, Bi, and alkali earth cations (when the B site contains transition metals with r_B = 0.5 to 0.7 Å).[4] With smaller cations at the A site, the perovskite structure becomes unstable (at ambient pressure), and other structural types are formed,[5] for example, the bixbyite structure ($ScFeO_3$)[6] and the hexagonal $YMnO_3$-type structure (h-$ScMnO_3$[7,8] and h-$InMnO_3$).[9]

There has been increased interest in recent years in highly distorted or exotic perovskites in order to find new physical properties and effects and unusual behavior.[10] One way to obtain new exotic perovskites is to introduce small cations (such as Sc^{3+}, In^{3+}, Mn^{2+}, and others) into the A site. This can be done using the high-pressure, high-temperature preparation method; this method gave, for example, $ScVO_3$ (8 GPa),[11] $ScMnO_3$ (12.5 GPa),[12] $(In_{1-x}Mn_x)MnO_3$ ($^1/_9 \le x \le {}^1/_3$) (6 GPa),[13] $MnVO_3$ (4.5−8 GPa),[14,15] Mn_2FeSbO_6 (6 GPa),[16] and even Mn_2O_3 (~20 GPa)[17] perovskites and perovskite-related $LiNbO_3$-type compounds, $(In_{1-x}M_x)MO_3$ (M = $Mn_{0.5}Fe_{0.5}$) (6 GPa)[18] and Mn_2FeNbO_6 (7 GPa).[19] $InCrO_3$ (6.5 GPa),[20] $InRhO_3$ (6.5 GPa),[20] and $ScCrO_3$ (4.5 GPa)[21] perovskites were first prepared long ago. However, only the lattice parameters of $InRhO_3$ were reported (a = 5.435 Å, b = 7.586 Å, and c = 5.301 Å),[20] and no information about its real crystal structure and properties is known.

In this work, we prepared $InRhO_3$ and a new perovskite $ScRhO_3$ and investigated their structural and magnetic properties. Both $ScRhO_3$ and $InRhO_3$ have a rare monoclinic superstructure of the $GdFeO_3$-type with lattice parameters of a = 7.45660 Å, b = 7.43524 Å, c = 7.52191 Å, and β = 93.2930(1)° (for $ScRhO_3$) and space group $P2_1/n$, and they are isostructural with the 1:3 B-site-ordered $Sr(Na_{0.25}Sb_{0.75})O_3$.[22] $InRhO_3$ has pseudo-orthorhombic lattice parameters. Therefore, their structures are different from the orthorhombic $GdFeO_3$-type structures of $RRhO_3$ perovskites (R represents rare-earth cations, Y, and Bi).[23−33] Both $InRhO_3$ and $ScRhO_3$ are nonmagnetic, similar to the $RRhO_3$ perovskites (R = Y, La, Sm, Lu, and Bi).[30,33]

2. EXPERIMENTAL SECTION

$ScRhO_3$ and $InRhO_3$ were prepared from stoichiometric mixtures of In_2O_3 (99.99%), Sc_2O_3 (99.9%), and Rh_2O_3 (99.9%). The mixtures (corresponding to the total weight of about 0.45 g for each compound) were placed in Au capsules and treated at 6 GPa in a belt-type high-pressure apparatus at 1500 K for 2 h. (The heating rate to the desired temperature was 10 min.) After heat treatment, the samples were quenched to room temperature (RT), and the pressure

Received: July 9, 2013
Published: September 30, 2013

dx.doi.org/10.1021/ic401760m | Inorg. Chem. 2013, 52, 12005−12011

Table 1. Structural Parameters of $ScRhO_3$ at Room Temperature[a]

site	Wyckoff position	x	y	z	B (Å^2)
Sc1	4*e*	0.20568(18)	0.2426(4)	0.77502(18)	0.44(3)
Sc2	4*e*	0.22445(19)	0.2328(3)	0.28865(18)	0.30(3)
Rh1	2*a*	0	0	0	0.22(3)
Rh2	2*b*	0	0	0.5	0.22(3)
Rh3	2*c*	0.5	0	0.5	0.34(3)
Rh4	2*d*	0.5	0	0	0.22(3)
O1	4*e*	0.2581(6)	0.4629(6)	0.6075(5)	0.22(9)
O2	4*e*	0.6021(6)	0.5481(6)	0.7545(6)	0.25(10)
O3	4*e*	0.1108(4)	0.2524(11)	0.0355(4)	0.10(10)
O4	4*e*	0.0416(6)	0.5982(6)	0.2525(7)	0.21(10)
O5	4*e*	0.4630(5)	0.2500(14)	0.8904(4)	0.45(7)
O6	4*e*	0.7533(7)	0.4074(6)	0.0469(6)	0.38(10)

[a]The occupation factor for all sites is unity. Space group $P2_1/n$ (No. 14; unique axis *b*, cell choice 2). $Z = 8$, $a = 7.45660(1)$ Å, $b = 7.43524(1)$ Å, $c = 7.52191(1)$ Å, $\beta = 93.2930(1)°$, and $V = 416.3385(9)$ Å^3. $R_{wp} = 4.61\%$, $R_p = 3.19\%$, $R_B = 1.19\%$, and $R_F = 0.80\%$. $\rho_{cal} = 6.249$ g/cm^3.

was slowly released. The resultant samples were dark-brown dense pellets.

X-ray powder diffraction (XRPD) data of $ScRhO_3$ and $InRhO_3$ were collected at RT on a Rigaku Ultima III diffractometer using Cu Kα radiation (2θ range of 10−100°, step width of 0.02°, and counting time of 10 s/step). Synchrotron XRPD data were measured at RT and 134 K on a large Debye−Scherrer camera at the BL15XU beamline of SPring-8.[34] The data were collected between 2 and 60° at a 0.003° interval in 2θ. The incident beam was monochromatized at 0.65297 Å. The samples were packed into Lindenmann glass capillaries (inner diameter 0.1 mm), which were rotated during the measurement. The absorption coefficient was measured. The Rietveld analysis was performed with RIETAN-2000.[35] For identified impurities, we refined only scale factors and lattice parameters, fixing their structural parameters.

Magnetic susceptibilities ($\chi = M/H$) of $ScRhO_3$ and $InRhO_3$ were measured on a SQUID magnetometer (Quantum Design, MPMS) between 2 and 300 K in different applied fields under both zero-field-cooled (ZFC) and field-cooled on cooling (FCC) conditions. Isothermal magnetization measurements were performed between 0 and 70 kOe at 5 and 300 K. All of the magnetization data were corrected for contributions from diamagnetic sample holders (obtained in separate experiments) and core diamagnetism ($\chi_{dia}/10^{-6} = -12.6$ (O^{2-}), −22 (Rh^{3+}), −6 (Sc^{3+}), and −19 (In^{3+}) cm^3/mol)[36] because negative total magnetization was observed at higher temperatures. The specific heat, $C_p(T)$, was measured from 300 to 2 K in a zero magnetic field by a pulse relaxation method using a commercial calorimeter (Quantum Design PPMS).

Differential scanning calorimetry (DSC) curves of $ScRhO_3$ (powder) and $InRhO_3$ (powder) were recorded on a Mettler Toledo DSC1 STAR^e system at a heating/cooling rate of 10 K/min between 293 and 873 K in open aluminum capsules. Two runs were performed to check the reproducibility. The first heating DSC curve showed sharp anomalies at 361 K in $ScRhO_3$ and at 406 K in $InRhO_3$. However, no anomalies were found on the first cooling curve and the second heating−cooling curves. XRPD measurements after the DSC experiments showed that the perovskite phases of $ScRhO_3$ and $InRhO_3$ remained unchanged. Therefore, the DSC anomalies on the first heating curve most probably originated from irreversible transformations in impurities or annealing effects.

3. RESULTS AND DISCUSSION

All reflections on synchrotron XRPD patterns with intensities above 1% were indexed using TREOR[37] in an orthorhombic system for $InRhO_3$ ($a = 5.4329$ Å, $b = 7.5837$ Å, and $c = 5.3003$ Å) and a monoclinic system for $ScRhO_3$ ($a = 5.4457$ Å, $b = 7.4353$ Å, $c = 5.1414$ Å, and $\beta = 90.5005°$). The orthorhombic lattice parameters of $InRhO_3$ were in very good agreement with the reported values.[20] The observed reflection conditions of $k + l = 2n$ for $0kl$ and $h = 2n$ for $hk0$ in $InRhO_3$ afforded two possible space groups, centrosymmetric *Pnma* (No. 62) and noncentrosymmetric $Pn2_1a$ (No. 33).[38] The structure parameters of $LuRhO_3$[33] in space group *Pnma* were used as the initial ones for the refinement of $InRhO_3$. Attempts to refine the structure of $InRhO_3$ in space group $Pn2_1a$ did not improve the fitting results. The observed reflection conditions of $k = 2n$ for $0k0$ in $ScRhO_3$ afforded two possible space groups, centrosymmetric $P2_1/m$ (No. 11) and noncentrosymmetric $P2_1$ (No. 4).[38] The structure parameters of Ca_2MnSbO_6[39] in space group $P2_1/m$ were used as the initial ones for the refinement of $ScRhO_3$. Attempts to refine the structure of $ScRhO_3$ in space group $P2_1$ did not improve the fitting results. Note that the initial substructure model for $ScRhO_3$ could also be deduced from the obtained structural parameters of $InRhO_3$ in *Pnma* by a group−subgroup transformation of *Pnma* > $P2_1/m$.

Good fits and reliable structural parameters were obtained in space group *Pnma* for $InRhO_3$ ($R_{wp} = 6.69\%$, $R_p = 4.71\%$, $R_B = 2.37\%$, and $R_F = 1.33\%$) and in space group $P2_1/m$ for $ScRhO_3$ ($R_{wp} = 5.92\%$, $R_p = 4.14\%$, $R_B = 3.63\%$, and $R_F = 2.13\%$) (Supporting Information). However, both samples contained many weak additional reflections. Some additional reflections in $InRhO_3$ were found to originate from InOOH and Rh impurities. Remaining additional reflections in $InRhO_3$ (except for three extremely weak reflections with $d = 2.880$, 2.822, and 1.995 Å) could be indexed in orthorhombic symmetry with the $\mathbf{2a} \times \mathbf{b} \times \mathbf{2c}$ superstructure. Many additional reflections in $ScRhO_3$ could be indexed in monoclinic symmetry with the $\pm(\mathbf{a} + \mathbf{c}) \times \mathbf{b} \times (\mathbf{a} - \mathbf{c})$ superstructure. However, some unindexed weak reflections remained in $ScRhO_3$; they could not be indexed in any reasonable superstructure. Therefore, they most probably originated from unknown impurities.

The $\pm(\mathbf{a} + \mathbf{c}) \times \mathbf{b} \times (\mathbf{a} - \mathbf{c})$ superstructure of the $P2_1/m$ substructure of $ScRhO_3$ can result in space groups $P2_1/m$ and $P2_1/n$ (the substructures and superstructures have group−subgroup relations with each other). Attempts to apply the $P2_1/m$ superstructure resulted in poor fitting of some superstructure reflections (actually two models with different origin shifts were checked). However, superstructure reflections could be perfectly fit with the $P2_1/n$ superstructure model. Therefore, the crystal structure of $ScRhO_3$ was refined in the $P2_1/n$ superstructure model. Note that there is another $P2_1/n$ superstructure model (with a different origin shift) where all sites are in general 4*e* positions. However, that model gave

dx.doi.org/10.1021/ic401760m | Inorg. Chem. 2013, 52, 12005−12011

larger R values and poor fitting of some superstructure reflections (Supporting Information).

Our attempts to construct an orthorhombic $2\mathbf{a} \times \boldsymbol{b} \times 2\mathbf{c}$ superstructure model for $InRhO_3$ [with a = 10.8658 Å, b = 7.5837 Å, and c = 10.6006 Å and maximum space group *Bmam* (standard setting is *Cmma*) or *Bmmm* (standard setting is *Cmmm*) based on the observed reflection conditions] failed. Attempts to solve the structure of $InRhO_3$ by direct methods with EXPO[40] in orthorhombic superstructures also failed. However, the structure of $InRhO_3$ could be solved with EXPO in space group $P2_1/n$ (where all Rh sites were in special centrosymmetric positions). Therefore, we used the obtained structural parameters of $ScRhO_3$ in space group $P2_1/n$ as the initial ones for the refinement of $InRhO_3$. All superstructure reflections of $InRhO_3$ could be perfectly fit with the $P2_1/n$ superstructure model. We note that the same situation was observed in $Sr(Na_{0.25}Sb_{0.75})O_3$,[22] where a substructure model was the *Pnma* $GdFeO_3$-type model (with $2^{1/2}a_p \times 2a_p \times 2^{1/2}a_p$ lattice parameters, where a_p is the parameter of the cubic perovskite subcell) and a superstructure model had $P2_1/n$ symmetry and $2a_p \times 2a_p \times 2a_p$ lattice parameters instead of orthorhombic symmetry and $2(2^{1/2})a_p \times 2a_p \times 2(2^{1/2})a_p$ lattice paremeters.

The refined structural parameters, R values, selected bond lengths, bond angles, and bond-valence sums (BVS)[41] of $ScRhO_3$ and $InRhO_3$ are listed in Tables 1–4. For $InRhO_3$, Table 2 gives structure parameters with fixed lattice parameters (obtained from the *Pnma* lattice parameters). This model gave more reliable Rh–O bond lengths. A model with the refined lattice parameters is given in the Supporting Information. Superstructure reflections were very weak in $InRhO_3$ (<0.5%, Supporting Information), probably originating from the ordering of oxygen atoms. $InRhO_3$ has heavy In and Rh atoms (in comparison to O atoms) and pseudo-orthorhombic lattice parameters. These facts could be the origin of less accurate localization of some oxygen atoms. In $ScRhO_3$, all Sc–O and Rh–O bond lengths were very reasonable, and BVS(Sc) and BVS(Rh) values were close to +3. Experimental, calculated, and difference synchrotron XRPD patterns are shown in Figure 1. Figure 2 depicts the crystal structure of $ScRhO_3$.

Table 2. Structural Parameters of $InRhO_3$ at Room Temperature[a]

site	Wyckoff position	x	y	z	B (Å^2)
In1	4*e*	0.2195(3)	0.2438(5)	0.7709(3)	0.26(3)
In2	4*e*	0.2298(3)	0.2341(2)	0.2780(4)	0.61(3)
Rh1	2*a*	0	0	0	0.37(7)
Rh2	2*b*	0	0	0.5	0.28(5)
Rh3	2*c*	0.5	0	0.5	0.30(6)
Rh4	2*d*	0.5	0	0	0.29(5)
O1	4*e*	0.2568(14)	0.4693(14)	0.5944(19)	0.51(4)
O2	4*e*	0.6005(18)	0.5505(15)	0.7479(13)	= B(O1)
O3	4*e*	0.1000(19)	0.2563(12)	0.0195(16)	= B(O1)
O4	4*e*	0.0377(18)	0.5886(18)	0.2483(14)	= B(O1)
O5	4*e*	0.4647(16)	0.2476(16)	0.8943(19)	= B(O1)
O6	4*e*	0.7587(14)	0.4025(16)	0.0353(18)	= B(O1)

[a]The occupation factor for all sites is unity. Space group $P2_1/n$ (No. 14; unique axis b, cell choice 2). Z = 8, a = 7.59020 Å, b = 7.58377 Å, c = 7.59010 Å, β = 91.4154°, and V = 436.770 Å^3. R_{wp} = 4.62%, R_p = 3.35%, R_B = 0.91%, and R_F = 0.70%. The weight fraction of Rh is 0.4%, and the weight fraction of InOOH is 0.1%. ρ_{cal} = 8.082 g/cm^3.

Table 3. Selected Bond Lengths (l (Å)), Bond Angles (deg), and Bond Valence Sums (BVS) in $ScRhO_3$[a]

Sc1–O5	2.061(4)	Sc2–O3	2.045(3)
Sc1–O6	2.094(5)	Sc2–O4	2.050(5)
Sc1–O1	2.117(5)	Sc2–O2	2.117(5)
Sc1–O3	2.122(3)	Sc2–O5	2.138(4)
Sc1–O4	2.191(5)	Sc2–O6	2.204(5)
Sc1–O1	2.270(5)	Sc2–O2	2.287(5)
Sc1–O2	2.711(5)	Sc2–O1	2.945(4)
Sc1–O6	2.935(5)	Sc2–O4	3.045(5)
BVS($Sc1^{3+}$)	2.91	BVS($Sc2^{3+}$)	2.89
Rh1–O1 (×2)	2.037(4)	Rh2–O6 (×2)	2.022(5)
Rh1–O2 (×2)	2.050(5)	Rh2–O5 (×2)	2.046(9)
Rh1–O3 (×2)	2.062(8)	Rh2–O2 (×2)	2.069(4)
BVS($Rh1^{3+}$)	2.98	BVS($Rh2^{3+}$)	3.02
Rh3–O6 (×2)	2.014(5)	Rh4–O4 (×2)	2.040(5)
Rh3–O3 (×2)	2.029(8)	Rh4–O5 (×2)	2.046(9)
Rh3–O4 (×2)	2.042(5)	Rh4–O1 (×2)	2.063(4)
BVS($Rh3^{3+}$)	3.16	BVS($Rh4^{3+}$)	2.98
Rh1–O2–Rh2 (×2)	131.9(1)	Rh2–O6–Rh3 (×2)	134.9(1)
Rh1–O3–Rh3 (×2)	130.7(1)	Rh2–O5–Rh4 (×2)	130.6(1)
Rh1–O1–Rh4 (×2)	130.8(1)	Rh3–O4–Rh4 (×2)	134.3(1)
		⟨Rh–O–Rh⟩	132.2

[a]BVS = $\Sigma_{i=1}^{N}\nu_i$, $\nu_i = \exp[(R_0 - l_i)/B]$, N is the coordination number, B = 0.37, $R_0(In^{3+})$ = 1.902, $R_0(Sc^{3+})$ = 1.849, and $R_0(Rh^{3+})$ = 1.791.[41]

Table 4. Selected Bond Lengths (l (Å)), Bond Angles (deg), and Bond Valence Sums (BVS) in $InRhO_3$

In1–O5	2.063(13)	In2–O2	2.093(11)
In1–O3	2.116(13)	In2–O4	2.095(13)
In1–O6	2.131(12)	In2–O3	2.180(13)
In1–O1	2.195(11)	In2–O6	2.217(14)
In1–O1	2.325(14)	In2–O5	2.221(14)
In1–O4	2.330(16)	In2–O2	2.379(14)
In1–O2	2.838(15)	In2–O1	2.995(14)
In1–O6	3.062(15)	In2–O4	3.065(15)
BVS($In1^{3+}$)	2.96	BVS($In2^{3+}$)	2.88
Rh1–O1 (×2)	2.010(11)	Rh2–O5 (×2)	2.090(13)
Rh1–O2 (×2)	2.049(11)	Rh2–O6 (×2)	2.109(10)
Rh1–O3 (×2)	2.091(10)	Rh2–O2 (×2)	2.112(10)
BVS($Rh1^{3+}$)	2.99	BVS($Rh2^{3+}$)	2.58
Rh3–O6 (×2)	1.999(11)	Rh4–O4 (×2)	2.052(11)
Rh3–O3 (×2)	2.002(10)	Rh4–O5 (×2)	2.057(12)
Rh3–O4 (×2)	2.015(11)	Rh4–O1 (×2)	2.073(11)
BVS($Rh3^{3+}$)	3.36	BVS($Rh4^{3+}$)	2.90
Rh1–O2–Rh2 (×2)	131.6(3)	Rh2–O6–Rh3 (×2)	134.9(3)
Rh1–O3–Rh3 (×2)	135.8(3)	Rh2–O5–Rh4 (×2)	132.2(3)
Rh1–O1–Rh4 (×2)	136.7(3)	Rh3–O4–Rh4 (×2)	137.9(3)
		⟨Rh–O–Rh⟩	134.9

Refinements of occupation factors (g) of cations together with all other structural parameters (listed in Tables 1 and 2), profile parameters, zero-shift parameters, and background parameters gave the following results. For $ScRhO_3$, g(Sc1) = 1.016(5) and g(Sc2) = 0.996(5) with fixed g(Rh1) = g(Rh2) = g(Rh3) = g(Rh4) = 1, and g(Rh1) = 0.991(5), g(Rh2) = 0.991(5), g(Rh3) = 0.986(5), and g(Rh4) = 0.991(5) with fixed g(Sc1) = g(Sc2) = 1. For $InRhO_3$, g(In1) = 1.004(3) and g(In2) = 0.996(3) with fixed g(Rh1) = g(Rh2) = g(Rh3) = g(Rh4) = 1, and g(Rh1) = 0.984(8), g(Rh2) = 1.019(8), g(Rh3) = 0.992(8), and g(Rh4) = 1.008(8) with fixed g(In1) =

dx.doi.org/10.1021/ic401760m | *Inorg. Chem.* 2013, 52, 12005–12011

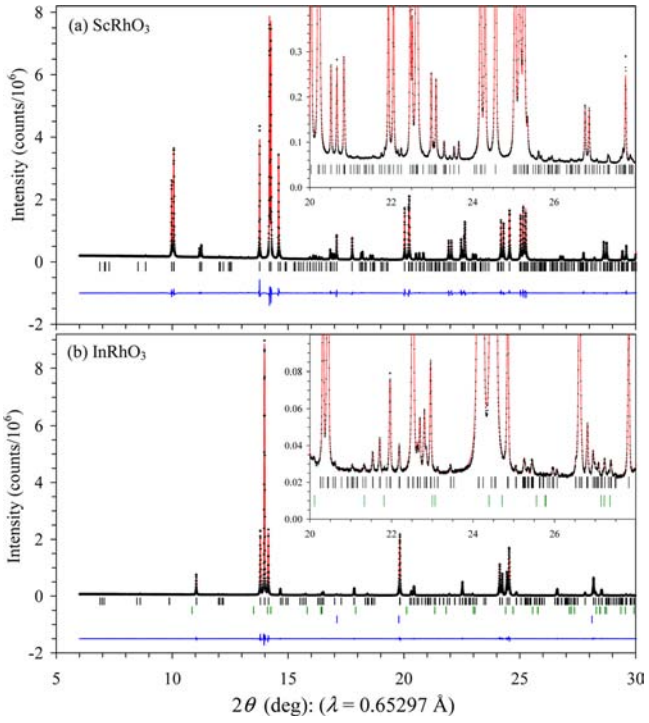

Figure 1. Portions (2θ = 6–30°) of experimental (black crosses), calculated (red line), and difference (blue line) synchrotron XRPD patterns of (a) $ScRhO_3$ and (b) $InRhO_3$. The bars show possible Bragg reflection positions for the perovskite phases (black bars) and InOOH (green bars) and Rh (blue bars) impurities in $InRhO_3$. Insets give enlarged images (2θ = 20–28°).

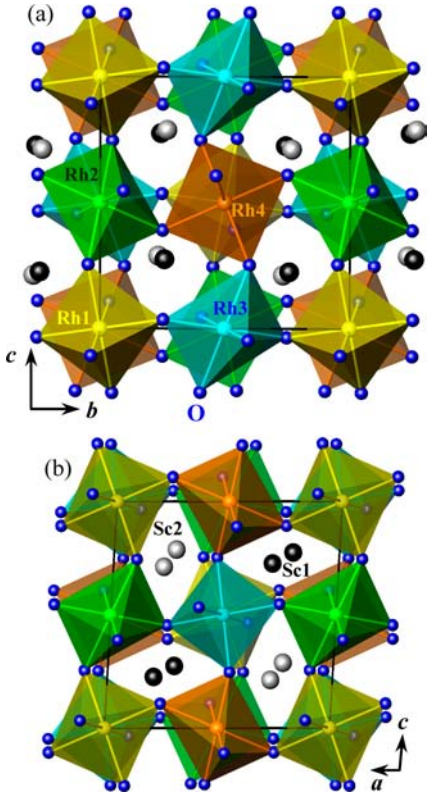

Figure 2. Crystal structure of $ScRhO_3$ along (a) the *a* axis and (b) the *b* axis.

g(In2) = 1. These results showed that the Sc/Rh ratio in $ScRhO_3$ and the In/Rh ratio in $InRhO_3$ were very close to 1:1.

Figure 3 shows the lattice parameters as a function of ionic radius (for 8-fold coordination)[4] for all $RRhO_3$ compounds (*R*

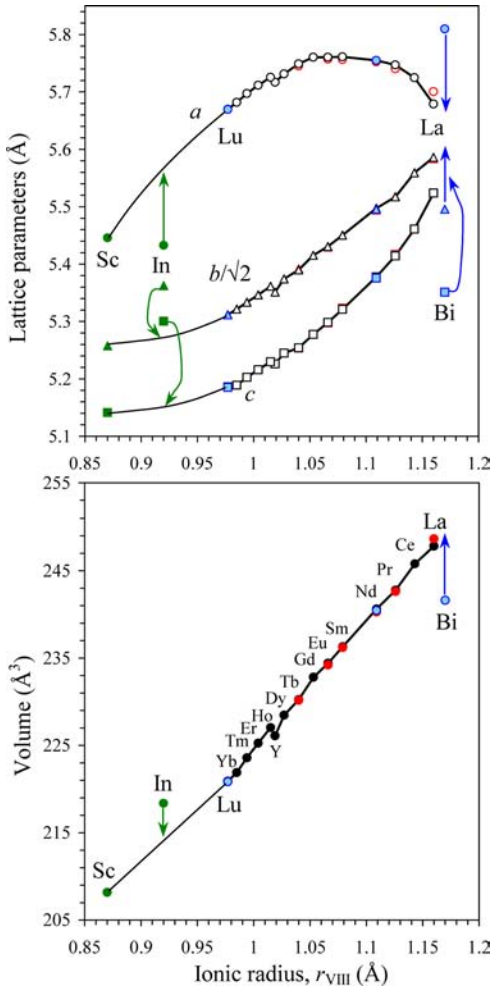

Figure 3. Lattice parameters and unit cell volume of $RRhO_3$ compounds (*R* = Sc, In, Y,[26] rare earths,[23,25–27,31,33] and Bi[33]) as a function of the ionic radius (in 8-fold coordination).[4] Arrows show the ideal lattice parameters for $InRhO_3$ and $BiRhO_3$ (or expected lattice parameters from the monotonic trends in the family).

= Sc, In, Y,[26] rare earths,[23,25–27,31,33] and Bi[33]). We used the lattice parameters of the substructure models for this figure. The lattice parameters and unit cell volume of $ScRhO_3$ follow the general monotonic behavior observed in $RRhO_3$ compounds (*R* = Y and La–Lu), but both $InRhO_3$ and $BiRhO_3$ exhibit a strong deviation from monotonic behavior. It is interesting that all lattice parameters and unit cell volumes for $InRhO_3$ and $BiRhO_3$ show opposite deviations from the expected values (which are based on the ionic radius). The peculiar behavior of both $InRhO_3$ and $BiRhO_3$ can be explained by the significant hybridization of In–O[42,43] and Bi–O bonds, resulting in more covalent bonds in comparison to *R*–O (*R* = Y and La–Lu) bonds. The same behavior of the lattice parameters was observed in $ScCrO_3$, $InCrO_3$, and $RCrO_3$ (*R* = Y and La–Lu) (Supporting Information).

The substructure of $InRhO_3$ has an orthorhombic $GdFeO_3$-type structure similar to that of the $RRhO_3$ perovskites (*R* is a rare earth cation, Y, or Bi).[23–33] The substructure of $ScRhO_3$

dx.doi.org/10.1021/ic401760m | Inorg. Chem. 2013, 52, 12005–12011

has a small monoclinic distortion of the $GdFeO_3$-type structure; this $P2_1/m$ distortion was observed in doped $CaMnO_3$-based manganites, $(Ca_{0.85}La_{0.15})MnO_3$,[44] $(Ca_{0.85}Tb_{0.15})MnO_3$,[45] $(Ca_{0.3}Nd_{0.7})MnO_3$,[46,47] $CaMn_{1-x}W_xO_3$,[48] and Ca_2MnSbO_6.[39] The *Pnma*-to-$P2_1/m$ transition in $CaMnO_3$-based manganites is often observed at low temperatures and associated with magnetic and charge ordering. We emphasize that the monoclinic angle in the substructure of $ScRhO_3$ is between the a ($= 2^{1/2}a_p$) and c ($= 2^{1/2}a_p$) lattice parameters. It is different from monoclinic angles between the $2^{1/2}a_p$ and $2a_p$ lattice parameters observed in B-site rock-salt-ordered perovskites.[16,49,50]

The superstructure found in both $ScRhO_3$ and $InRhO_3$ was observed only, to the best of our knowledge, in 1:3 B-site-ordered $Sr(Na_{0.25}Sb_{0.75})O_3$.[22] The tilt angles for each RhO_6 octahedron in $ScRhO_3$ and $InRhO_3$ can be calculated with equations given in ref 22, and the results can be found in the Supporting Information. However, for the purpose of comparison, we compare tilt angles of $ScRhO_3$ and $InRhO_3$ calculated for the substructure models with those of $RRhO_3$ perovskites (R is a rare earth cation, Y, or Bi).[23−33] The tilt system of *Pnma* is $a^+b^-b^-$ (ref 51) according to Glazer's notation.[52] The tilt system of $P2_1/m$ is similar, $a^+b^-c^-$.[51] The only difference is that the rotation along the c axis should not be the same as the rotation along the b axis. The tilt system of the $P2_1/n$ superstructure cannot be written in Glazer's notation, but the octahedral tilt system should be basically the same as that of the substructures.[22] A weak superstructure could appear from the independent tilting of octahedra in different layers (Figure 2b).

The octahedral tilt angles in *Pnma* can be estimated from the atomic coordinates of the O2 atom. We used the formulas for the tilt angles as defined in ref 53: in-phase tilt angle $\phi_{O2} = \arctan(1 + 2x_{O2} - 2z_{O2})$ and out-of-phase tilt angle $\varphi_{O2} = \arctan(2^{5/2}y_{O2})$ (for our coordinates in space group *Pnma*). The out-of-phase tilt angle can also be calculated from the atomic coordinates of the O1 atom: $\varphi_{O1} = \arctan(2^{3/2}z_{O1})$.[54] A tilt angle can be calculated from the lattice parameters, $\phi_{lattice} = \arccos(2^{1/2}c^2/(ab))$.[55] Figure 4 shows different tilt angles as a function of ionic radius (for 8-fold coordination)[4] for all $RRhO_3$ compounds (R = Sc, In, Y,[26] rare earths,[23,25−27,31,33] and Bi[33]). In-phase tilt angle ϕ_{O2} monotonically increases with decreasing the R^{3+} ionic radius (except for $BiRhO_3$). Out-of-phase tilt angles φ_{O2} and φ_{O1} are close to each other (again except for $BiRhO_3$) with an anomaly from the monotonic behavior on $InRhO_3$. Tilt angle $\phi_{lattice}$ shows strong anomalies in $InRhO_3$ and $BiRhO_3$ because of their anomalous lattice parameters (Figure 3).

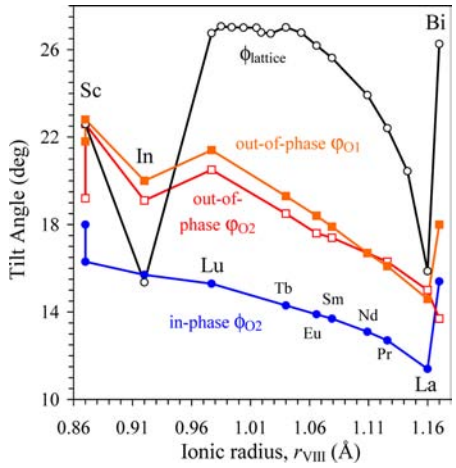

Figure 4. Different tilt angles as a function of the ionic radius (in 8-fold coordination) in $RRhO_3$ compounds (R = Sc, In, Y, rare earths,[31,33] and Bi[33]). See the text for definitions of the tilt angles.[53−55]

All tilt angles of $ScRhO_3$ were larger that those of $InRhO_3$ (Figure 4 and Supporting Information). This is an expected result because $ScRhO_3$ with smaller Sc^{3+} ions at the A site should have larger distortions. However, the difference in tilt angles is not very significant, and the oxygen coordination of Sc^{3+} and In^{3+} ions is similar in $ScRhO_3$ and $InRhO_3$ with six short bond lengths and two much longer bond lengths (Tables 3 and 4).

The Goldschmidt tolerance factor of $ScRhO_3$ is 0.735, and that of $InRhO_3$ is 0.753 (with the ionic radius for 6-fold coordination). Therefore, $ScRhO_3$ and $InRhO_3$ should not be stable at ambient pressure.[3] The high-pressure, high-temperature method is needed to stabilize them under ambient conditions. So far, $ScVO_3$,[11] $ScCrO_3$,[10,21] $ScMnO_3$,[12] $ScRhO_3$, $InCrO_3$,[10,20] $(In_{1-x}Mn_x)MnO_3$,[13] and $InRhO_3$ simple perovskites could be prepared by the high-pressure, high-temperature method. $ScVO_3$, $ScCrO_3$, and $InCrO_3$ crystallize in the *Pnma* $GdFeO_3$-type structure ($2^{1/2}a_p \times 2a_p \times 2^{1/2}a_p$) at RT with one crystallographic site for V^{3+} and Cr^{3+}. $ScMnO_3$ crystallizes in the B-site-ordered $GdFeO_3$-type structure with space group $P2_1/n$ ($2^{1/2}a_p \times 2^{1/2}a_p \times 2a_p$)[12] similar to $(In_{1-x}Mn_x)MnO_3$ ($^1/_9 \le x \le {}^1/_3$)[13] with two crystallographic Mn sites having quite different Jahn−Teller distortions. $ScRhO_3$ and $InRhO_3$ have the most complicated superstructure of the original $GdFeO_3$-type structure with space group $P2_1/n$ ($2a_p \times 2a_p \times 2a_p$) among $ScMO_3$ and $InMO_3$ compounds. For $ScRhO_3$, small Sc^{3+} ions at the A site and strong bending of the $-RhO_6-RhO_6-$ chains (with the average ⟨Rh−O−Rh⟩ bond angle of 132.2°) should contribute to its unusual structural distortion. Bond angles are larger in $ScVO_3$ (⟨V−O−V⟩ = 136.5°),[11] $ScCrO_3$ (⟨Cr−O−Cr⟩ = 137.9°),[10] and $ScMnO_3$ (⟨Mn−O−Mn⟩ = 135.0°).[12] In-phase tilt angle ϕ_{O2} is the largest in $ScRhO_3$ and $InRhO_3$ among known $ScMO_3$ and $InMO_3$ compounds (Supporting Information).

Synchrotron XRPD data at 134 K (a = 7.45257(1) Å, b = 7.43103(1) Å, c = 7.51929(1) Å, and β = 93.2603(1)° for $ScRhO_3$; a = 5.42927(2) Å, b = 7.57701(2) Å, and c = 5.29713(1) Å in *Pnma* and a = 7.58254(3) Å, b = 7.57701(1) Å, c = 7.58786(1) Å, and β = 91.4115(1)° in $P2_1/n$ for $InRhO_3$) showed that the crystal symmetry of $ScRhO_3$ and $InRhO_3$ did not change. Specific heat measurements between 2 and 300 K (Figure 5) and DSC measurements between 293 and 873 K also showed no anomalies. All of these facts indicate the absence of low-temperature phase transitions and high-temperature phase transitions up to 873 K in $ScRhO_3$ and $InRhO_3$. We note that specific heat measurements by the pulse relaxation method sometimes cannot detect structural phase transitions, for example, in $PbPd_2O_4$.[56]

The specific heat between 5 and 19 K for $ScRhO_3$ and 3 and 19 K for $InRhO_3$ could be fit by the equation (inset of Figure 5)

$$C_p(T) = \gamma T + \beta_1 T^3 + \beta_2 T^5 \quad (1)$$

where the first term is associated with the electronic contribution and the second and third terms describe the lattice contribution. The fitted parameters were γ = 0.52(4) mJ/mol K^2, β_1 = 0.0589(5) mJ/mol K^4, and β_2 = 2.88(14) ×

dx.doi.org/10.1021/ic401760m | *Inorg. Chem.* 2013, 52, 12005−12011

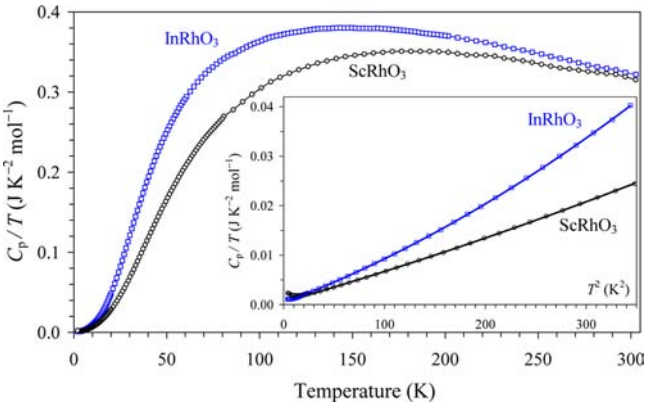

Figure 5. Specific heat data of $ScRhO_3$ (black circles) and $InRhO_3$ (blue squares) at zero magnetic field plotted as C_p/T vs T (lines are drawn for eye). The inset gives the C_p/T vs T^2 curves (symbols) with the fitting results by eq 1 (lines).

10^{-5} mJ/mol K^6 for $ScRhO_3$ and $\gamma = 0.387(15)$ mJ/mol K^2, $\beta_1 = 0.0778(3)$ mJ/mol K^4, and $\beta_2 = 1.107(8) \times 10^{-4}$ mJ/mol K^6 for $InRhO_3$. The existence of the γT term with very small values of the γ coefficient could originate from the presence of impurities (such as metallic Rh in $InRhO_3$). The values of β_1 gave Debye temperatures, $\Theta_D = (234Nk_B/\beta_1)^{1/3}$ (N is Avogadro's number and k_B is Boltzmann's constant), of 320 K for $ScRhO_3$ and 292 K for $InRhO_3$, which are comparable to the Debye temperatures of other perovskites: $BiRhO_3$ ($\Theta_D \approx$ 236 K),[33] $LuRhO_3$ ($\Theta_D \approx$ 271 K),[33] and $SrVO_3$ ($\Theta_D \approx$ 322 K).[57]

Figure 6 shows the χ versus T curves of $ScRhO_3$ and $InRhO_3$ at 50 kOe and M versus H curves at 5 and 300 K. There was basically no difference between the ZFC and FCC curves. No anomalies were observed on the χ versus T curves, and the curves could be fit with the equation

$$\chi(T) = \chi_0 + \frac{0.125\mu_{eff}^{\ 2}}{T - \theta} \qquad (2)$$

where χ_0 is a temperature-independent term, μ_{eff} is the effective magnetic moment in the Bohr magneton μ_B, and θ is the Curie–Weiss temperature. The fitting parameters were $\chi_0 = 6.48(9) \times 10^{-5}$ cm^3/mol, $\mu_{eff} = 0.173(1)\mu_B$/f.u., and $\theta = -5.4(1)$ K for $ScRhO_3$ and $\chi_0 = 5.64(9) \times 10^{-5}$ cm^3/mol, $\mu_{eff} = 0.155(2)\mu_B$/f.u., and $\theta = -7.8(3)$ K for $InRhO_3$. Similar effective magnetic moments were observed in $RRhO_3$ (R = La, Lu, and Bi).[30,33] The small effective magnetic moments suggest that the weak magnetism of $ScRhO_3$ and $InRhO_3$ comes from traces of paramagnetic impurities or defects. $ScRhO_3$ and $InRhO_3$ are nonmagnetic, and this is in agreement with the nonmagnetic low-spin state of Rh^{3+} ions (t^6_{2g}).

In conclusion, we prepared $InRhO_3$ and new perovskite $ScRhO_3$ and investigated their structural and magnetic properties. Both $InRhO_3$ and $ScRhO_3$ are nonmagnetic similar to the $RRhO_3$ perovskites (R = Y, La, Sm, Lu, and Bi),[30,33] and they show no phase transitions between 2 and 873 K. From this point of view, they are not very interesting in comparison to similar compounds $ScMO_3$ and $InMO_3$ containing other transition metals. However, they have a rare superstructure of the $GdFeO_3$-type with space group $P2_1/n$ and lattice parameters $2a_p \times 2a_p \times 2a_p$. Therefore, exotic perovskites with small cations at the A site continue to provide interesting structural or physical properties.

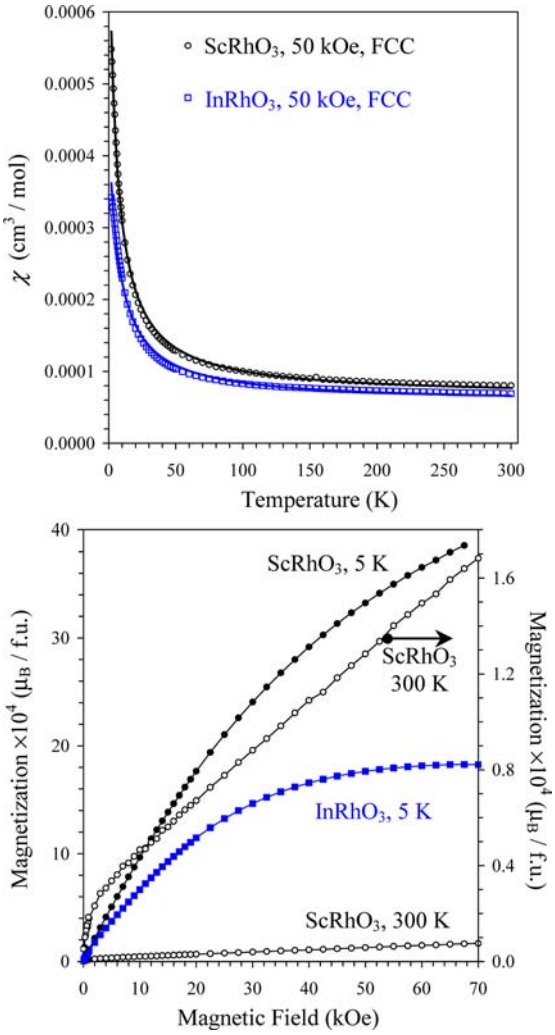

Figure 6. (Top) χ vs T curves of $ScRhO_3$ (black circles) and $InRhO_3$ (blue squares) at 50 kOe in the field-cooled regime on cooling. Lines show fitting results with eq 2. (Bottom) M vs H curves for $ScRhO_3$ at 5 K (black circles) and 300 K (white circles, right- and left-hand axes) and for $InRhO_3$ at 5 K (blue squares). Lines are drawn to guide the eye.

■ ASSOCIATED CONTENT

Ⓢ Supporting Information

Structural parameters of $ScRhO_3$ and $InRhO_3$ in different structural models, fitting results, laboratory X-ray powder diffraction patterns, additional structural figures, DSC curves, tilt angle calculations, lattice parameters, and unit cell volumes of $RCrO_3$ (R = Sc, In, Y, and La–Lu) compounds. This material is available free of charge via the Internet at http://pubs.acs.org.

■ AUTHOR INFORMATION

Corresponding Author

*E-mail: alexei.belik@nims.go.jp.

Notes

The authors declare no competing financial interest.

■ ACKNOWLEDGMENTS

This work was supported by the World Premier International Research Center Initiative (WPI Initiative, MEXT, Japan), the Japan Society for the Promotion of Science (JSPS) through its

Funding Program for World-Leading Innovative R&D on Science and Technology (FIRST Program), and Grants-in-Aid for Scientific Research (22246083 and 21540330) from JSPS, Japan. The synchrotron radiation experiments were performed at SPring-8 with the approval of the Japan Synchrotron Radiation Research Institute (proposal numbers 2011B4512 and 2012A4507). We thank Dr. A. M. Abakumov for consultations related to superstructures in perovskites.

REFERENCES

(1) Mitchell, R. H. *Perovskites: Modern and Ancient*; Almaz Press: Thunder Bay, Ontario, Canada, 2002.
(2) Goldschmidt, V. M. *Naturwissenschaften* **1926**, *21*, 477.
(3) Eitel, R. E.; Randall, C. A.; Shrout, T. R.; Rehrig, P. W.; Hackenberger, W.; Park, S. E. *Jpn. J. Appl. Phys. Part 1* **2001**, *40*, 5999.
(4) Shannon, R. D. *Acta Crystallogr., Sect. A* **1976**, *32*, 751.
(5) Giaquinta, D. M.; zur Loye, H.-C. *Chem. Mater.* **1994**, *6*, 365.
(6) Breard, Y.; Fjellvag, H.; Hauback, B. *Solid State Commun.* **2011**, *151*, 223.
(7) Bieringer, M.; Greedan, J. E. *J. Solid State Chem.* **1999**, *143*, 132.
(8) Uusi-Esko, K.; Malm, J.; Imamura, N.; Yamauchi, H.; Karppinen, M. *Mater. Chem. Phys.* **2008**, *112*, 1029.
(9) Yu, T.; Gao, P.; Wu, T.; Tyson, T. A.; Lalancette, R. *Appl. Phys. Lett.* **2013**, *102*, 172901.
(10) Belik, A. A.; Matsushita, Y.; Tanaka, M.; Takayama-Muromachi, E. *Chem. Mater.* **2012**, *24*, 2197.
(11) Castillo-Martinez, E.; Bieringer, M.; Shafi, S. P.; Cranswick, L. M. D.; Alario-Franco, M. A. *J. Am. Chem. Soc.* **2011**, *133*, 8552.
(12) Chen, H. Y.; Yu, T.; Gao, P.; Bai, J. M.; Tao, J.; Tyson, T. A.; Wang, L.; Lalancette, R. *Inorg. Chem.* **2013**, *52*, 9692.
(13) Belik, A. A.; Matsushita, Y.; Tanaka, M.; Takayama-Muromachi, E. *Angew. Chem., Int. Ed.* **2010**, *49*, 7723.
(14) Syono, Y.; Akimoto, S. I.; Endoh, Y. *J. Phys. Chem. Solids* **1971**, *32*, 243.
(15) Markkula, M.; Arevalo-Lopez, A. M.; Kusmartseva, A.; Rodgers, J. A.; Ritter, C.; Wu, H.; Attfield, J. P. *Phys. Rev. B* **2011**, *84*, 094450.
(16) Mathieu, R.; Ivanov, S. A.; Solovyev, I. V.; Bazuev, G. V.; Kumar, P. A.; Lazor, P.; Nordblad, P. *Phys. Rev. B* **2013**, *87*, 014408.
(17) Ovsyannikov, S. V.; Abakumov, A. M.; Tsirlin, A. A.; Schnelle, W.; Egoavil, R.; Verbeeck, J.; Van Tendeloo, G.; Glazyrin, K. V.; Hanfland, M.; Dubrovinsky, L. *Angew. Chem., Int. Ed.* **2013**, *52*, 1494.
(18) Belik, A. A.; Furubayashi, T.; Yusa, H.; Takayama-Muromachi, E. *J. Am. Chem. Soc.* **2011**, *133*, 9405.
(19) Li, M.-R.; Walker, D.; Retuerto, M.; Sarkar, T.; Hadermann, J.; Stephens, P. W.; Croft, M.; Ignatov, A.; Grams, C. P.; Hemberger, J.; Nowik, I.; Halasyamani, P. S.; Tran, T. T.; Mukherjee, S.; Dasgupta, T. S.; Greenblatt, M. *Angew. Chem., Int. Ed.* **2013**, *52*, 8406.
(20) Shannon, R. D. *Inorg. Chem.* **1967**, *6*, 1474.
(21) Park, J. H.; Parise, J. B. *Mater. Res. Bull.* **1997**, *32*, 1617.
(22) Alonso, J. A.; Mzayek, E.; Rasines, I. *J. Solid State Chem.* **1990**, *84*, 16.
(23) (a) Wold, A.; Post, B.; Banks, E. *J. Am. Chem. Soc.* **1957**, *79*, 6365. (b) Wold, A.; Arnott, R. J.; Croft, W. J. *Inorg. Chem.* **1963**, *2*, 972.
(24) Chazalon, R.; Bertaut, E. F.; Duc, T. Q. *Bull. Soc. Fr. Mineral. Cristallogr.* **1964**, *87*, 98.
(25) Shannon, R. D. *Acta Crystallogr., Sect. B* **1970**, *26*, 447.
(26) Lazarev, V. B.; Shaplygin, I. S. *Russ. J. Inorg. Chem.* **1978**, *23*, 1449; *Zh. Neorg. Khim.* **1978**, *23*, 2614.
(27) Shaplygin, I. S.; Lazarev, V. B. *Russ. J. Inorg. Chem.* **1978**, *23*, 626; *Zh. Neorg. Khim.* **1978**, *23*, 1131.
(28) Kochergina, L. L.; Fomichev, V. V.; Kondratov, O. I.; Shaplygin, I. S.; Petrov, K. I. *Russ. J. Inorg. Chem.* **1980**, *25*, 1153; *Zh. Neorg. Khim.* **1980**, *25*, 2082.
(29) Jarrett, H. S.; Sleight, A. W.; Kung, H. H.; Gillson, J. L. *J. Appl. Phys.* **1980**, *51*, 3916.
(30) Taniguchi, T.; Iizuka, W.; Nagata, Y.; Uchida, T.; Samata, H. *J. Alloys Compd.* **2003**, *350*, 24.
(31) Macquart, R. B.; Smith, M. D.; zur Loye, H. C. *Cryst. Growth Des.* **2006**, *6*, 1361.
(32) Longo, J. M.; Raccah, P. M.; Kafalas, J. A.; Pierce, J. W. *Mater. Res. Bull.* **1972**, *7*, 137.
(33) Yi, W.; Liang, Q. F.; Matsushita, Y.; Tanaka, M.; Hu, X.; Belik, A. A. *J. Solid State Chem.* **2013**, *200*, 271.
(34) Tanaka, M.; Katsuya, Y.; Yamamoto, A. *Rev. Sci. Instrum.* **2008**, *79*, 075106.
(35) Izumi, F.; Ikeda, T. *Mater. Sci. Forum* **2000**, *321−324*, 198.
(36) Bain, G. A.; Berry, J. F. *J. Chem. Educ.* **2008**, *85*, 532.
(37) Werner, P. E.; Eriksson, L.; Westdahl, M. *J. Appl. Crystallogr.* **1985**, *18*, 367.
(38) *International Tables for Crystallography*, 5th ed.; Hahn, T., Ed.; Kluwer: Dordrecht, The Netherlands, 2002; Vol. *A*, p 52.
(39) Mandal, T. P.; Poltavets, V. V.; Croft, M.; Greenblatt, M. *J. Solid State Chem.* **2008**, *181*, 2325.
(40) Altomare, A.; Burla, M. C.; Camalli, M.; Carrozzini, B.; Cascarano, G. L.; Giacovazzo, C.; Guagliardi, A.; Moliterni, A. G. G.; Polidori, G.; Rizzi, R. *J. Appl. Crystallogr.* **1999**, *32*, 339.
(41) Brese, N. E.; O'Keeffe, M. *Acta Crystallogr., Sec. B* **1991**, *47*, 192.
(42) Oak, M. A.; Lee, J. H.; Jang, H. M.; Goh, J. S; Choi, H. J.; Scott, J. F. *Phys. Rev. Lett.* **2011**, *106*, 047601.
(43) Kumagai, Y.; Belik, A. A.; Lilienblum, M.; Leo, N.; Fiebig, M.; Spaldin, N. A. *Phys. Rev. B* **2012**, *85*, 174422.
(44) Pissas, M.; Kallias, G.; Hofmann, M.; Toebbens, D. M. *Phys. Rev. B* **2002**, *65*, 064413.
(45) Blasco, J.; Ritter, C.; Garcia, J.; de Teresa, J. M.; Perez-Cacho, J.; Ibarra, M. R. *Phys. Rev. B* **2000**, *62*, 5609.
(46) Millange, F.; Caignaert, V.; Mather, G.; Suard, E.; Raveau, B. *J. Solid State Chem.* **1996**, *127*, 131.
(47) Richard, O.; Schuddinck, W.; Van Tendeloo, G.; Millange, F.; Hervieu, M.; Caignaert, V.; Raveau, B. *Acta Crystallogr., Sect. A* **1999**, *55*, 704.
(48) Miclau, M.; Hejtmanek, J.; Retoux, R.; Knizek, K.; Jirak, Z.; Fresard, R.; Maignan, A.; Hebert, S.; Hervieu, M.; Martin, C. *Chem. Mater.* **2007**, *19*, 4243.
(49) King, G.; Thimmaiah, S.; Dwivedi, A.; Woodward, P. M. *Chem. Mater.* **2007**, *19*, 6451.
(50) King, G.; Woodward, P. M. *J. Mater. Chem.* **2010**, *20*, 5785.
(51) Howard, C. J.; Stokes, H. T. *Acta Crystallogr. Sect., B* **1998**, *54*, 782.
(52) Glazer, A. M. *Acta Crystallogr., Sect. B* **1972**, *28*, 3384.
(53) Kennedy, B. J.; Hovard, C. J.; Chakoumakos, B. C. *J. Phys.: Condens. Matter* **1999**, *11*, 1479.
(54) Abrashev, M. V.; Backstrom, J.; Borjesson, L.; Popov, V. N.; Chakalov, R. A.; Kolev, N.; Meng, R. -L.; Iliev, M. N. *Phys. Rev. B* **2002**, *65*, 184301.
(55) O'Keeffe, M.; Hyde, B. *Acta Crystallogr., Sect. B* **1977**, *33*, 3802.
(56) Yi, W.; Matsushita, Y.; Tanaka, M.; Belik, A. A. *Inorg. Chem.* **2012**, *51*, 7650.
(57) Inoue, I. H.; Goto, O.; Makino, H.; Hussey, N. E.; Ishikawa, M. *Phys. Rev. B* **1998**, *58*, 4372.